EXPERIMENTAL VALIDATION OF HIGH SPEED HAZARD AVOIDANCE CONTROL FOR UNMANNED GROUND VEHICLES

Matthew Spenko, Steven Dubowsky, and Karl Iagnemma

E-mail: mspenko@stanford.edu
Massachusetts Institute of Technology, Department of Mechanical Engineering
Cambridge, MA, 02139

Abstract: At high speeds in natural terrain, unmanned ground vehicles can experience unexpected situations that require rapid hazard avoidance maneuvers. In these scenarios there is often limited time to replan a path based on high-order dynamic models. This paper presents a novel method for high speed navigation and hazard avoidance based on the two dimensional "trajectory space," a compact and computationally efficient model-based representation of a robot's dynamic performance limits on natural terrain. This paper also presents a novel method for trajectory replanning, based on a "curvature matching" technique. Experimental results on a small high-speed UGV demonstrate the method's effectiveness. *Copyright © 2005 IFAC*

Keywords: Autonomous Mobile Robots, Obstacle Avoidance.

1. INTRODUCTION AND LITERATURE REVIEW

There are many important military, disaster relief, and surveillance applications that require a unmanned ground vehicle (UGV) to move at high speeds through uneven, natural terrain with various compositions and physical parameters (Gerhart, 1999; Walker 2001). Often a UGV is directed to follow a pre-planned path (or navigate through pre-defined waypoints) designated by an off-line mission-level planning algorithm. However, in natural terrain at high speeds, it is likely that dangerous and unexpected situations will occur. These may be the result of outdated topographical data, unidentified hazards due to sensor limitations or errors, or unanticipated physical terrain conditions. In these situations a UGV must quickly execute a maneuver that allows it to safely avoid the impending hazard. Despite increasing computing power, at high speeds there is little time to perform navigation based on detailed dynamic vehicle and terrain models.

Hazard avoidance has been traditionally performed either by selecting from a set of predetermined paths (i.e. search techniques over small spaces), or by reactive (reflexive) behaviors, which evoke a predetermined action in response to specific sensor signals. Many of these techniques have been designed for use on flat or slightly rolling terrain, at speeds that do not excite vehicle dynamics. Here the problem of navigation and hazard avoidance on flat, rough, and uneven terrain at speeds that excite the vehicle's dynamics is addressed.

Previous researchers have addressed this problem with a search-based technique to navigate a HMMWV-class vehicle at speeds up to 10 m/s while avoiding large hazards (Coombs, *et al*., 2000). The method relies on a pre-computed database of approximately 1.5×10^7 clothoidal paths. Since the vehicle is assumed to travel on relatively flat terrain at fairly low speeds, the model used in the calculations does not consider vehicle dynamics. An online algorithm eliminates candidate clothoids that intersect with hazards or are not feasible given the initial steering conditions. From the remaining path, the algorithm chooses one that follows the most benign terrain. Several contenders of the 2005 DARPA Grand Challenge utilize similar approaches which have proven to be successful for speeds in excess of 8 m/s. However, the techniques do not

consider the important aspects of terrain roughness, inclination, and vehicle/terrain traction characteristics, all of which will become increasingly more important as autonomous vehicles move from traversing roads and relatively benign terrain to more dangerous and extreme topography.

Researchers have developed a fuzzy logic-based algorithm for reactive outdoor hazard avoidance (Daily, et al., 1988; Olin, et al., 1991). The approach arbitrates between hazard avoidance and goal seeking and allows for UGV navigation at speeds up to 1 m/s. Another successful reactive behavior-based technique was developed where the "behaviors" are candidate steering angles, and an arbitrator chooses a steering angle based on hazard and goal locations (Kelly and Stentz, 1998). Other work in the area has focused on problems arising from partially known and dynamic environments (Laugier, et al., 1998) or sensing issues in outdoor terrains (Langer, et al., 1994). Although these techniques have been successful at low to moderate speeds, they do not explicitly consider vehicle dynamics and changing terrain characteristics.

In this paper, a hazard avoidance method that considers vehicle dynamics, terrain parameters, and hazard properties is experimentally validated. It is computationally efficient enough for high-speed applications. The work has similarities to the dynamic window method for low-speed collision avoidance in structured environments (Fox, et al., 1997). The technique described here incorporates features that are critical to UGV navigation, such as vehicle/terrain interaction, the presence of hazards, and terrain roughness and unevenness. The algorithm relies on the trajectory space, a compact framework for analyzing a UGV's dynamic performance on uneven, natural terrain (Spenko, et al., 2004). In addition, an algorithm is presented here for trajectory replanning after a hazard avoidance maneuver has been enacted. Here, the effectiveness of the proposed hazard avoidance and replanning algorithms is demonstrated through experimental results of a UGV moving at high speeds over flat and sloped terrain. It is shown that the algorithms operate favorably in harsh, real world conditions.

1. PROBLEM STATEMENT AND ASSUMPTIONS

Here the problem of high speed UGV hazard avoidance in natural terrain is addressed. "High speed" is loosely defined as speeds that induce vehicle dynamic effects including wheel slip, sideslip, roll-over, and ballistic motion. Hazards are defined as discrete objects or terrain features that significantly impede or halt UGV motion, such as trees, boulders, or patches of very soft soil. Hazards are assumed to be detected from on-board range sensors. Hazard detection and sensing issues are not a focus of this work.

The UGV is assumed to be following a pre-planned path derived from coarse map data. The goal of the algorithm is to rapidly plan maneuvers that permit the UGV to avoid unexpected hazards while considering

vehicle dynamics, steering dynamics, vehicle/terrain interaction, and vehicle performance limits. After the hazard avoidance maneuver is complete, the algorithm must efficiently resume the nominal path, again considering the above factors.

A terrain patch is described by its average roll (ϕ), pitch (ψ), roughness (ϖ), and traction coefficient (μ). It is assumed that coarse estimates of the tire/ground traction coefficient and ground roughness are known or can be determined online. Techniques for measuring or estimating the above parameters are available (Dudgeon and Gopalakrishnan, 1996; Iagnemma and Dubowsky, 2004). It is also assumed that vehicle inertial and kinematic properties are known with reasonable uncertainty. The vehicle is assumed to be equipped with a range sensor for measuring terrain elevation and locating hazards up to 30 vehicle lengths ahead, an inertial navigation sensor that can measure the vehicle's roll, pitch, yaw, and a global positioning system for measuring vehicle position.

2. TRAJECTORY SPACE DESCRIPTION

The hazard avoidance algorithm is based on the trajectory space, a two-dimensional space of a vehicle's instantaneous path curvature, κ, and longitudinal velocity, v. Fig. 1 shows an illustration of the trajectory space with icons depicting a vehicle's actions corresponding to various points in the space.
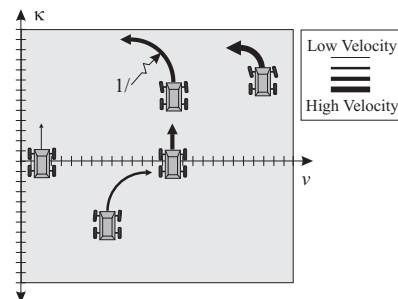

Fig. 1: Representation of vehicle action as described by its location in the trajectory space.

The trajectory space is a convenient space for navigation for two reasons. First, constraints can be imposed on the space to yield a compact representation of a vehicle's critical performance limits over uneven terrain. These constraints include dynamic roll over, side slip, steering mechanism limits, over/understeer, and acceleration, braking, and steering rate limits. Second, the trajectory space maps easily to the UGV actuation space (generally consisting of the throttle/brake and steering angle). This section provides a very brief summary of the application of the trajectory space to UGV navigation. A more complete description can be found elsewhere (Spenko 2005).

2.1. The Dynamic Trajectory Space, A

The dynamic trajectory space consists of curvature and velocity pairs (v, κ) that do not cause excessive

side slip or rollover and are attainable considering vehicle steering effects (i.e. over/understeer).

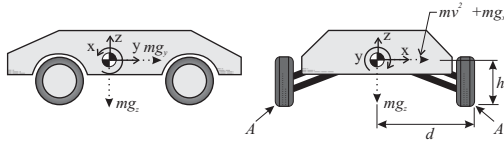As an example, rollover constraints can be calculated using the low-order model shown in Fig. 2.

Fig. 2: Low-order rollover model

For a UGV with a wheelbase greater than its track width, rollover most commonly occurs when the moment about either of the points *A* in Fig. 2 is equal to zero. Thus the constraint function for the rollover space can be defined as:

$$\kappa_{rollover}^{max,min} = \frac{dg_z \pm hg_x}{hv^2} \qquad (1)$$

where *d* is one half the axle length, *h* is the center of mass height, and *v* is the UGV's longitudinal velocity. The two solutions correspond to upslope/downslope travel. Constraints for side slip and steering effects can be derived from similarly low-order models. Details are presented in Spenko, 2005.

Fig. 3 illustrates the effect of terrain inclination on the dynamic trajectory space rollover limits. This example corresponds to a HMMVW-class vehicle traversing a side slope of 30 deg with the fall line perpendicular to the vehicle's heading. As expected the vehicle can safely execute downhill turns (negative curvature) with greater velocity than it can execute uphill turns due to the interacting effects of gravity and centripetal acceleration.
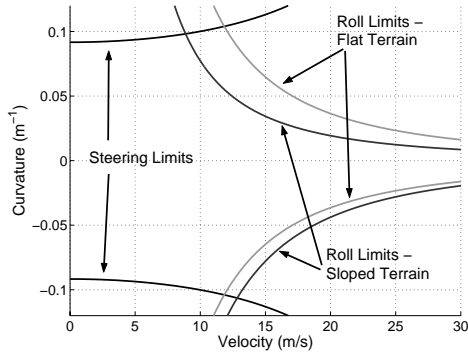

Fig. 3: Dynamic trajectory space limits for varying terrain roll angles (UGV wheelbase = 2.5 m).

2.2. The Reachable Trajectory Space, B

The reachable trajectory space consists of velocity and curvature pairs that can be transitioned to in a finite time *t*. It is a function of the current UGV curvature and velocity as well as actuator, acceleration, braking, and steering characteristics. Fig. 4 shows a sample reachable trajectory space overlaid on the dynamic trajectory space for a HMMWV size vehicle with a current location in the trajectory space of $(v = 20.0, \kappa = 0.01)$. Steering rate

limits are here fixed such that $\dot{\kappa}_{max} = 0.05$. Details of computation of *B* are given in Spenko, 2005.
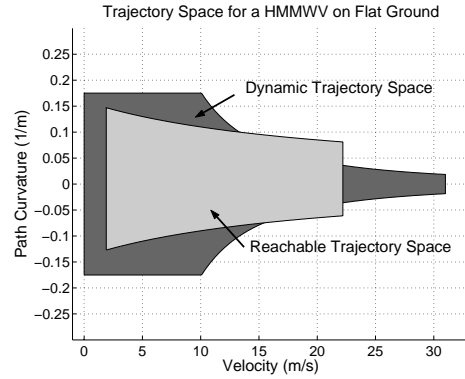

Fig. 4: Reachable trajectory space

2.3. The Admissible Trajectory Space, N

The admissible trajectory space (ATS) consists of the intersection of the dynamic trajectory space and the reachable trajectory space, i.e. $N = A \cap B$.

2.4. The Hazard Trajectory Space, H

The hazard trajectory space consists of curvatures and velocities that, if maintained from the current UGV position, would lead to intersection with a hazard (see Fig. 5). Here a point vehicle representation is employed.
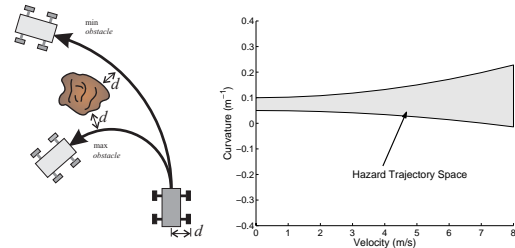

Fig. 5: Illustration of hazard trajectory space.

3. HIGH SPEED HAZARD AVOIDANCE

During high-speed navigation, emergency situations are likely to occur that require a UGV to rapidly perform a hazard avoidance maneuver. The two fundamental issues are 1) hazard detection, and 2) hazard avoidance maneuver selection. These are discussed below.

3.1. Hazard Detection

Here a scenario similar to that illustrated in Fig. 6 is assumed. A UGV attempts to follow a pre-planned nominal trajectory given by a high-level path planner, $\tau_{nominal} \equiv (v(\mathbf{x}), \kappa(\mathbf{x}))$, where $\mathbf{x}$ designates the UGV position in space. If the hazard detected by an onboard range sensor poses a threat, the UGV enacts an emergency hazard avoidance maneuver. The sensor scan is divided into *n* discrete vehicle-sized patches and an ATS corresponding to each patch is computed. The size and number of these patches, sensor accuracy, and throughput are important issues, but are beyond the scope of this paper.
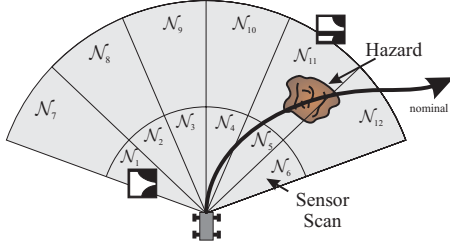
Fig. 6: ATSs defined with hazard present.

Let N_i denote the ATS for a patch that $\tau_{nominal}$ intersects. Let N_{traj} be defined as the intersection of all N_i, i.e. $N_{traj} \equiv N_1 \cap ... \cap N_m$, where m is the number of patches that $\tau_{nominal}$ intersects. A maneuver is enacted when a hazard lies on the vehicle's current desired path or when a part of $\tau_{nominal}$ will violate a constraint on N_{traj} (i.e. a UGV is commanded to follow a dynamically inadmissible trajectory for a given terrain).

3.2. Hazard Avoidance Maneuver Selection

To determine which maneuver to enact, let the total admissible trajectory space be defined as the intersection of all ATSs in the sensor scan minus the hazard space, H:

$$N_{total} \equiv (N_1 \cap ... \cap N_n) - H \qquad (2)$$

Let τ describe the UGV velocity and curvature at the current position $\mathbf{x}$. The goal of hazard avoidance is to find $\tau^*(\mathbf{x}) \mid \tau^*(\mathbf{x}) \in N_{total}$ where τ^* represents the hazard avoidance maneuver. The maneuver thus transitions the vehicle from a location that violates an ATS constraint to one that does not violate a constraint on any patch in the surrounding terrain. There are numerous techniques for finding a τ^* that results in a "good" maneuver. The following method was adopted for its simplicity.

First, the trajectory space is discretized into i closely spaced grid points. τ^* is chosen as the location in the trajectory space that minimizes the distance, Δ, from the current location in the trajectory space, $\tau = (v_0, \kappa_0)$, to a candidate point:

$$\Delta = \sqrt{\frac{K_1}{\kappa_{max} - \kappa_{min}}(\kappa_0 - \kappa_i) + \frac{K_2}{v_{max}}(v_0 - v_i)} \qquad (3)$$

where K_1 and K_2 are static non-negative gain factors. These factors affect the relative weighting of changes in velocity and curvature. The minimum distance Δ over N_{total} can be found using a variety of search techniques.

The resulting τ^* represents a dynamically admissible curvature and velocity pair that avoids hazards in the current sensor scan. A low-level control algorithm is then employed to command the UGV along the new trajectory.

4. PATH RESUMPTION

After a hazard avoidance maneuver is executed, the UGV must plan a kinematically and dynamically feasible path to return to the pre-planned nominal path. Assuming constant velocity, v, the state of a front-steered rear-drive wheeled vehicle can be described by the following coupled nonlinear equations.

$$\kappa(s) = u(s) \qquad \theta(s) = v \int_0^L \kappa(s)ds$$

$$x(s) = v \int_0^L \cos\theta(s)ds \qquad y(s) = v \int_0^L \sin\theta(s)ds \qquad (4)$$

where s represents the vehicle distance along a path, $u(s)$ is the steering input, and $\theta(s)$ is the vehicle heading angle.

Consider the situation illustrated by the plot shown in Fig. 7. Here the solid line represents a pre-planned nominal maneuver's curvature in path coordinates. A hazard avoidance maneuver is executed at a, and the maneuver ends at b. The curvature of the nominal desired path, hazard avoidance maneuver, and path resumption maneuver are defined as $\kappa_1(s)$, $\kappa_2(s)$, and $\kappa_3(s)$ respectively. The goal of the path replanning problem is to find $\kappa_3(s)$ in a computationally efficient manner such that:

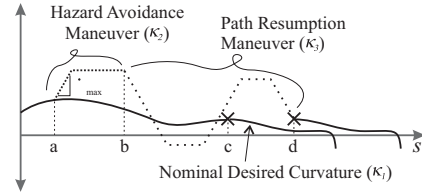$$(\kappa(c), \theta(c), x(c), y(c))_1 = (\kappa(d), \theta(d), x(d), y(d))_3 \quad (5)$$

Fig. 7: Curvature diagram

where c is the desired "meeting point" of the replanning maneuver and the nominal trajectory, and d is the terminal point of the replanning maneuver.

A computationally efficient replanning method termed the 'curvature matching method' is presented here. An outline of the method is presented below:

1. Make an initial choice of the "meeting point" on the nominal trajectory. Here c is initially chosen such that $(c - b) = (b - a)$. The initial value of d is chosen to be the smallest value such that it is possible to transition from $\kappa_2(b)$ to $\kappa_3(d)$ without violating $|\dot{\kappa}| \le \dot{\kappa}_{max}$

2. Find $\kappa_3(s)$ such that:

$$\int_a^c \kappa_1(s)ds = \int_a^b \kappa_2(s)ds + \int_b^d \kappa_3(s)ds \qquad (6)$$

This ensures that $\theta_1(c) = \theta_3(d)$. The curvature, κ_3, must also stay within the boundaries of the total admissible trajectory space. Details of this computation are given in (Spenko, 2005).

3. Calculate $x_3(d)$ and $y_3(d)$ using (4).

4. If $x_3(d)$ and $y_3(d)$ are within the acceptable threshold the algorithm ends. If not, c and d are adjusted as:

$$c_{i+1} = c_i - k_c(e_{lon})$$
$$d_{i+1} = d_i - k_d(e_{lat}) \qquad (7)$$

where k_c and k_d are adjustable gains and e_{lon} and e_{lat} are the longitudinal and lateral error respectively and are defined by:

$$e_{lon} = (x_1(c) - x_3(d))\cos\theta_1(c) + (y_1(c) - y_3(d))\sin\theta_1(c)$$
$$e_{lat} = (x_3(d) - x_1(c))\sin\theta_1(c) + (y_1(c) - y_3(d))\cos\theta_1(c)$$
$$(8)$$

Although algorithm convergence cannot be formally guaranteed, extensive analysis has shown that the method performs well in practice (Spenko, 2005).

5. EXPERIMENTAL RESULTS

Extensive experimental trials of the hazard avoidance maneuver were conducted on the Autonomous Rough Terrain Experimental System (ARTEmiS) shown in Fig. 8. ARTEmiS measures 0.88l x 0.61w x 0.38h m and has 0.25 m diameter pneumatic tires. It is equipped with a 2.5 Hp Zenoah G2D70 gasoline engine, Crossbow AHRS-400 inertial navigation system (INS), Novatel DGPS capable of 0.2 meter resolution, Futaba S5050 servos for steering, brakes, and throttle, and a PIII 700 MHz PC104 computer. ARTEmiS is not equipped with forward-looking range sensors. Instead, using knowledge of ARTEmiS' position, hazard locations are revealed once they are within the range of a "virtual sensor."

Fig. 8: ARTEmiS experimental UGV

5.1. Experimental Validation of Trajectory Space Constraints

The accuracy of the trajectory space roll over constraints was studied experimentally on flat terrain at speeds up to 8 m/s (see Fig. 9). The vehicle was commanded on a desired path consisting of a straight line followed by a clothoid segment. Roll over was defined as occurring when $a_y \geq gh/d$, where a_y is the lateral acceleration of the vehicle, g is gravity, h is the height of the vehicle center of mass and d is one-half the axle width. This simple metric is commonly used for rollover studies in the passenger vehicle industry. Due to the high traction coefficient ($\mu \approx 1.3$), roll over occurred before excessive side slip.

The experimental data matches the predicted dynamic limit well. The most prevalent source of error is the calculation of the path curvature, which can be highly sensitive to the GPS and INS position estimates.
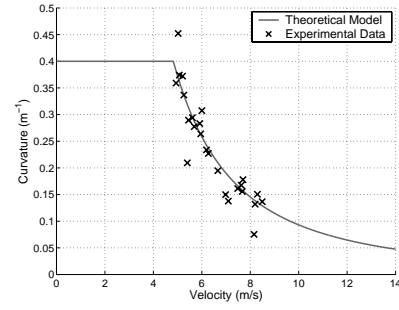
Fig. 9: Experimentally validated trajectory space constraints for flat ground

5.2. High Speed Multiple Hazard Avoidance

Fig. 10 shows three "snapshot" subplots of an experiment for high speed avoidance of two hazards performed on a grass field at 6 m/s. The nominal desired path was a straight path 100 m long. The first hazard was detected at $x = 16.4\,\text{m}$, shown in the top subplot of Fig. 10. At this point hazard avoidance and path resumption maneuvers were executed. ARTEmiS followed the modified path until a second hazard was detected at $x = 34.1\,\text{m}$, shown in the middle subplot of Fig. 10. A second maneuver was executed and ARTEmiS successfully completed the path, as shown in the lower section of Fig. 10.
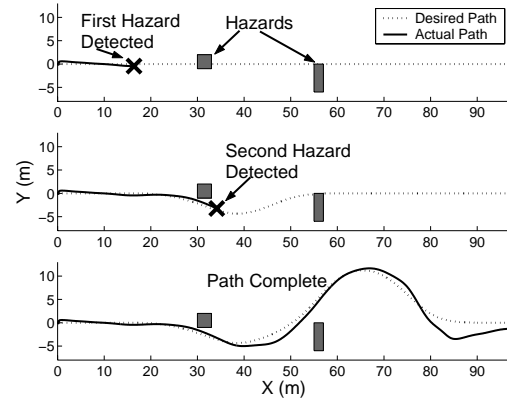
Fig. 10: Experimental results of hazard avoidance maneuvers executed for multiple hazards

Fig. 11 shows the trajectory spaces at the two instants that the hazards were detected. The asterisks depict ARTEmiS' location in the trajectory space. For the first hazard, ARTEmiS modified its trajectory from $\tau = (6.0, 0.00)$ to $\tau = (6.0, -0.03)$. For the second hazard ARTEmiS modified its trajectory by maintaining its current location inside the trajectory space until beyond the hazard.
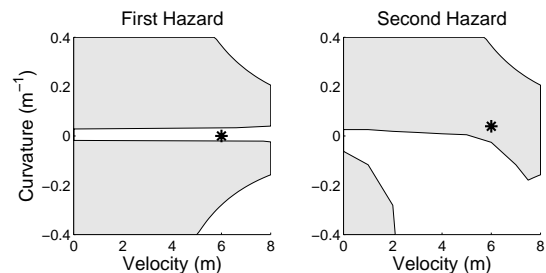
Fig. 11: Trajectory spaces at time of hazard detection

5.3. Hazard Avoidance on Rough Terrain

Experiments on rough terrain were performed at Minute Man National Historic Park (see Fig. 12). The terrain consisted of a bumpy, uncut grass field with features on the order of one-half the wheel radius. The nominal desired path is a 100 m long straight path. The hazard consists of a cluster of tall brushes, and small trees. Terrain roughness influences UGV mobility by inducing variation in the wheel normal forces. This can be represented as variation in the location of trajectory space constraints (Spenko, 2005).
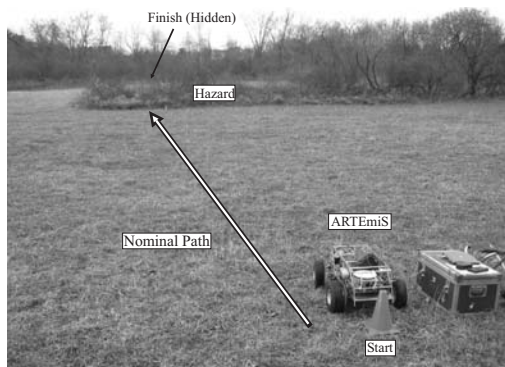

Fig. 12: Rough terrain experimental setup.

Fig. 13 shows three "snapshot" subplots of the experiment performed at a speed of 7.0 m/s. ARTEmiS detected the first hazard at $x = 10.4\,\mathrm{m}$. This is shown in the top subplot of Fig. 13. At this point hazard avoidance and path resumption maneuvers were executed, as shown in the middle subplot of Fig. 13. The lower section of Fig. 13 shows the completed path.
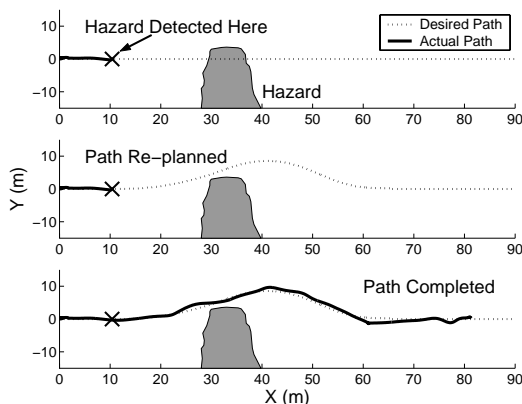

Fig. 13: Rough terrain experimental results.

This experiment demonstrates that the proposed hazard avoidance algorithm can be applied to UGVs operating at high speeds on rough terrain. These conditions are expected to be similar to actual operating conditions for many practical applications.

The above results are representative of a body of experimental studies that have been performed to analyze the performance of the proposed algorithm. Generally, it has been observed that the algorithm quickly and effectively generates dynamically safe emergency hazard avoidance maneuvers for UGVs traveling a high speeds. The algorithm has been experimentally tested for over 80 hours at speeds ranging from 4-9 m/s. It has been validated on flat and rough terrain with slopes up to 18 degrees.

6. CONCLUSIONS

This paper has presented experimental validation of a novel hazard avoidance algorithm for high-speed UGVs in natural terrain. A brief description of the trajectory space was presented, which describes UGV performance limits on uneven terrain. This information was used as the basis of a hazard avoidance algorithm. A computationally efficient path resumption algorithm was also presented. Experimental results demonstrate the effectiveness of the algorithms.

REFERENCES

Coombs, D., et al. (2000). Driving autonomously off-road up to 35 km/h. *Proc. of the IEEE Intelligent Vehicle Symposium*, 186-191.

Daily, M. et al. (1988). Autonomous cross-country navigation with the ALV. *Proceedings of the IEEE ICRA*, **2,** 718-726.

Dudgeon, J. and R. Gopalakrishnan (1996) Fractal-based modeling of 3D terrain surfaces. *Proc. of the IEEE Conf. on Bringing Together Education, Science, and Technology*, 246-252.

Fox, D., W. Burgard, and S. Thrun, (1997) The dynamic window approach to collision avoidance. *IEEE Robotics and Automation*, **23**, 23-33.

Iagnemma, K., and S. Dubowsky (2004) *Mobile Robots in Rough Terrain, STAR Series on Advanced Robotics*, Springer.

Kelly, A., and A. Stentz. (1998) Rough terrain autonomous mobility – part 1: a theoretical analysis of requirements. *Autonomous. Robots* **5** 129-161.

Langer, D., J.K. Rosenblatt, and M. Hebert. (1994) A behavior-based system for off-road navigation. *IEEE Robotics and Automation*, **10.6,** 776-783.

Laugier, C. et al. (1998) Sensor-based control architecture for a car-like vehicle. *Proc. of IEEE ICRA* 216-222.

Olin, K. and D. Tseng, (1991) Autonomous cross-country navigation: an integrated perception and planning system." *IEEE Expert*, **6.4,** 16- 30.

Spenko, M., K. Iagnemma, and S. Dubowsky, (2004) High speed hazard avoidance for mobile robots in rough terrain. *Proc. of SPIE Unmanned Ground Vehicle Technology VI*, **5422**

Spenko, M. (2005) Hazard Avoidance for High-Speed Rough-Terrain Unmanned Ground Vehicles *Ph.D. Thesis. Massachusetts Institute of Technology*.